nature communications

Article

https://doi.org/10.1038/s41467-023-42956-2

Cryo-EM structure of TMEM63C suggests it functions as a monomer

Received: 8 July 2023

Accepted: 26 October 2023

Published online: 09 November 2023

Check for updates

Yuqi Qin[1,8], Daqi Yu[1,8], Dan Wu[2,8], Jiangqing Dong[1,8], William Thomas Li[1], Chang Ye[2], Kai Chit Cheung[1], Yingyi Zhang[3], Yun Xu[2], YongQiang Wang[4] ✉, Yun Stone Shi[2,5] ✉ & Shangyu Dang[1,6,7] ✉

The TMEM63 family proteins (A, B, and C), calcium-permeable channels in animals that are preferentially activated by hypo-osmolality, have been implicated in various physiological functions. Deficiency of these channels would cause many diseases including hearing loss. However, their structures and physiological roles are not yet well understood. In this study, we determine the cryo-electron microscopy (cryo-EM) structure of the mouse TMEM63C at 3.56 Å, and revealed structural differences compared to TMEM63A, TMEM63B, and the plant orthologues OSCAs. Further structural guided mutagenesis and calcium imaging demonstrated the important roles of the coupling of TM0 and TM6 in channel activity. Additionally, we confirm that TMEM63C exists primarily as a monomer under physiological conditions, in contrast, TMEM63B is a mix of monomer and dimer in cells, suggesting that oligomerization is a regulatory mechanism for TMEM63 proteins.

The response of cells to both internal and external mechanical stimulation is critical for living organisms to adapt to and survive in their environments. The mechanosensitive ion channels (MSCs) are responsible for cellular mechanotransduction, a process that converts mechanical force to electrical and ion flux signals upon receiving mechanical stimulations including physical force and osmotic pressure[1,2]. Several types of MSCs have been identified[3], including the bacterial MscS, and MscL channels[4–8], TREK/TRAAK two-pore domain potassium channels (K2P)[9,10], Piezo1/2 non-selective cation channels[11–13], NompC/TRPN from transient receptor potential (TRP) superfamily[14–18], epithelial sodium channel/degenerin/acid-sensing (ENaC/DEG/ASIC) superfamily ion channels[19,20], TMC1/2[21–23], and TMEM63/OSCA[24,25].

TMEM63s, together with its plant orthologues OSCAs, are members of a newly identified OSCA/TMEM63 cation channel family that are activated by mechanical forces of osmolality[24,25]. OSCAs are characterized as calcium-permeable channels sensing hyperosmotic stress and influencing water transpiration regulation and root growth in plants[26], and several structures about OSCA are available[25,27–29]. Different from OSCAs, TMEM63s calcium influx is preferentially activated by hypo-osmolality in animals[30], and none of the TMEM63 structures were determined. Though remotely related in protein sequences to members of transmembrane protein 16 (TMEM16), the OSCA/TMEM63 family proteins share similar 3-dimensional (3D) architectures with TMEM16s[31–33]. Furthermore, TMC[34] also resembles structures of TMEM16s. Based on the structural similarities, TMC, OSCA/TMEM63 and TMEM16 are grouped into the TMEM16 superfamily with diverse functions[3]. In previous studies, structural investigations have consistently demonstrated that TMEM16s[31–33], TMC[34,35], and OSCAs[25,27–29] adopt a dimeric assembly, with each monomer containing a single ion permeation pore. Although the exact mechanism remains unclear, these structural observations strongly suggest that dimerization is a common characteristic among TMEM16 superfamily proteins.

[1]Division of Life Science, The Hong Kong University of Science and Technology, Clear Water Bay, Hong Kong, China. [2]State Key Laboratory of Pharmaceutical Biotechnology, Department of Neurology, Nanjing Drum Tower Hospital Affiliated to Medical School, Nanjing University, Nanjing 210032, China. [3]Biological Cryo-EM Center, The Hong Kong University of Science and Technology, Clear Water Bay, Kowloon, Hong Kong, China. [4]Howard Hughes Medical Institute, University of California, San Francisco, CA 94158, USA. [5]Guangdong Institute of Intelligence Science and Technology, Hengqin, Zhuhai 519031, China. [6]Southern Marine Science and Engineering Guangdong Laboratory (Guangzhou), Guangzhou, China. [7]HKUST-Shenzhen Research Institute, Nanshan, Shenzhen 518057, China. [8]These authors contributed equally: Yuqi Qin, Daqi Yu, Dan Wu, Jiangqing Dong. ✉e-mail: yongqiang.wang@ucsf.edu; shiyun@gdiist.cn; sdang@ust.hk

TMEM63 has three members, TMEM63A, B and C in most animals including mouse and human. In Drosophila, only one type of TMEM63 is identified that senses humidity[36] and food grittiness[37]. Mouse TMEM63s, and human TMEM63A were reported to induce stretch-activated currents when expressed in naïve cells[24]. According to clinical and genome-wide association studies, heterozygous missense mutations of human TMEM63A (G168E, I462N, and G567S) are linked to an infantile disorder, showing similar symptoms resembling hypomyelination leukodystrophy[38]. In support, cells transfected with these disease-related variants in TMEM63A did not generate stretch-activated currents[38]. TMEM63B plays an important role in maintaining auditory function in mouse outer hair cells (OHCs)[30]. In addition, overexpressed TMEM63B in HEK293T cells can enhance cell migration and wound healing[39]. The increased level of TMEM63B mRNA expression detected in ductal carcinoma T47-D human tumor cell line suggests that TMEM63B may also serve as cancer biomarker[39]. TMEM63C is essential for maintaining the kidney filtration barrier integrity in zebrafish, and expresses low in chronic kidney disease patients[40].

Despite these clinical and experimental observations, studies of TMEM63s are hampered by the lack of structure information and physiological roles. Here, we determine the 3.56-Å structure of mouse TMEM63C by using single-particle cryo-electron microscopy (cryo-EM), which works as a monomer in cells. This cryo-EM structure, in combination with structure-guided mutagenesis and functional analysis, allows us to establish the structural mechanisms and the physiological functions of TMEM63. Three bulky conserved pore-facing residues in TMEM63B/C act as a gate for channel activity, while the coupling between TM0 and TM6 facilitates the opening of the channel for ion transport. These observations provide valuable insights into understanding the mechanisms of the OSCA/TMEM63 family, as well as other members of the TMEM16 superfamily.

Results

Overall structure of TMEM63C

The full-length mouse TMEM63C was overexpressed in HEK293S cells. Target protein was solubilized and purified in the detergent n-Dodecyl-β-d-maltoside (DDM), followed by exchange into lauryl maltose neopentyl glycol (LMNG) for structural studies (Supplementary Fig. 1a). Using single-particle cryo-EM, we determined the structure of TMEM63C at 3.56 Å resolution as a monomer (Fig. 1a, b, Supplementary Figs. 1b–d, 2, 3 and Supplementary Table 1). Local resolution analysis revealed a higher resolution in the transmembrane regions and a lower resolution in the intracellular regions, suggesting the dynamic of intracellular regions (Supplementary Fig. 3a). TMEM63C contains 11 transmembrane helices (TMs), TM0-TM10. The N-terminus is oriented towards the extracellular space, while the C-terminus faces the cytosol (Fig. 1c). Between TM2 and TM3, there is a long cytosolic domain mainly formed by α-helices (Fig. 1c). TM3 and TM4 are tilted to the membrane, and situated at the outer boundary of the transmembrane region (Fig. 1a, b). A short α-helix is linked to the intracellular region of TM6 and TM7 separately. TM7 and TM8 are shorter that do not extend the whole membrane (Fig. 1).

Despite the monomeric TMEM63C observed in the cryo-EM map, the overall structure of TMEM63C resembles OSCA, its plant orthologue. mTMEM63C and atOSCA1.1 (PDB:6JPF)[25] exhibit a sequence identity of 21.6% for the full length (Supplementary Figs. 8, 9), while transmembrane region RMSD (root mean square deviation) is 1.25 Å for pruned pairs and 3.77 Å for all pairs. TMEM63C and OSCA consist of 11 transmembrane α-helices spanning from TM0 to TM10 with conserved structures. Additionally, the intracellular soluble domain of both proteins is primarily composed of the region between TM2 and TM3, as well as the C-terminus.

Besides a similar fold, some differences still exist in the pore region of TMEM63C and OSCA. Particularly, the short α-helix located at the cytoplasmic side of TM6 (TM6b) swung to TM4 to avoid the clash with TM0 (Supplementary Fig. 4a, b), the intracellular half of which moved close to TM6, compared to that in OSCA. The movement of TM6b may narrow the ion-passing pore of TMEM63C for calcium entrance[41]. Other pore-forming helices, including the TM5 and TM7, also shifted slightly, thereby contributing to a different pore profile of TMEM63C (Supplementary Fig. 4c).

Using pore-forming helices as reference, structural alignment of TMEM63C and OSCA indicated the major differences come from helices surrounding the pore region (Supplementary Fig. 4). The extracellular side of the TM2 adopted a shift to TM10. Consequently, two neighboring helices, TM9 and TM10, were pushed away rigidly. On the other hand, the cytoplasmic side of TM7 slightly shifted to TM1, and pushed it away from the pore region. The conformational differences of these pore-region surrounding helices may sense membrane distortion introduced by mechanical forces, and convert it to intracellular signal by regulating channel activity. In OSCA, TM2 and TM10 face the dimer interface and connect to the dimer interaction intracellular domain. These morphological differences in TM2 and TM10 might also contribute to oligomerization state variation between TMEM63C and OSCA.

Pore profile of TMEM63C

Similar to OSCA, the ion-passing pore of TMEM63C is surrounded by TM3-7. The Caver program[42] was used to measure the radii of the pore region. The results show that TMEM63C is in closed state with two restriction sites, the radii of which is smaller than 1 Å (Fig. 2a, b). Three bulky pore-facing residues (F542, F543 and Y546 on TM6) (Fig. 2d, Supplementary Fig. 5a), highly conserved among TMEM63 and OSCA (Fig. 2c), have been proposed to play critical roles in channel activities[25]. To test this hypothesis, we examined the channel activity of TMEM63C by combining functional assays and mutagenesis. Expectedly, compared to wild type TMEM63C, alanine substitution of F542, F543 and Y546 all resulted in an increased channel activity, reflected by the higher percentage of responding cells and maximal Ca^{2+} rise (Fig. 2e, f). The results of calcium imaging further demonstrated three highly conserved bulky residues play important roles in channel gating. Under normal conditions, three bulky hydrophobic resides, localized at the entry site of the ion passing pore, prevent access of the hydrophilic calcium ions. Once hypotonic condition is achieved, these residues may point away from ion passing pore as a consequence of TM6 rotation.

Coupling of TM0 and TM6 is important for TMEM63C channel activity

TMEM63C undergoes a conformational change in TM6 that leads to the broadening of the pore for calcium entry in response to hypotonic stress. However, the mechanism of how TMEM63C senses hypotonic stress to open the pore is unclear. Interestingly, lysine substitution of V39 on TM0, Q451 and S455 on TM4, and N545 on TM6 all elevated the ratio of responding cells and maximal Ca^{2+} rise in TMEM63C (Fig. 2g–i, Supplementary Fig. 5b). These residues are not facing pore region, the substitution of lysine, a relatively bulky positive charged residue, may either cause rotation of pore helices, like TM6, or destabilize the pore region, to avoid steric repulsion, therefore increasing the opening probability of TMEM63C.

Previously, MD simulation and mutagenesis results suggested that TM6 and TM0 may couple together to trigger the opening of the pore in OSCA upon mechanical stimuli[25]. To test if this mechanism could be applied to TMEM63C, we performed cysteine substitution of V39 on TM0 and N545 on TM6, two residues are spatially close to each other based on the structural observation. TMEM63C variants with single mutation (V39C, N545C) presented a higher activity than wild type. Moreover, double mutant (V39C and N545C), forming more stringent coupling between TM0 and TM6 with disulfide bond, produced the

https://doi.org/10.1038/s41467-023-42956-2

highest activity (Fig. 2h, i). Unsurprisingly, in the presence of the reducing agent, DTT, the channel activity of this double mutant TMEM63C significantly decreased, probably due to the release of the tight binding between TM0 and TM6. In contrast, the channel activity of the wild type or single mutant (N545C) TMEM63C remained unchanged upon DTT treatment (Fig. 2j, k). These results suggested coupling of TM0 and TM6 may play an important role in channel opening in responding to the hypotonic environment.

TMEM63B shares similar working mechanism with TMEM63C

To verify whether the mechanism of hypotonic stress response and pore opening can be applied to other members of the TMEM63 family, mouse TMEM63B was introduced. Relatively high sequence similarity (44% identity and 63% similarity) of TMEM63B and TMEM63C suggested that the structure of TMEM63B should resemble that of TMEM63C (Supplementary Figs. 8, 9). Therefore, the homology model of TMEM63B was generated based on sequence alignment and atomic

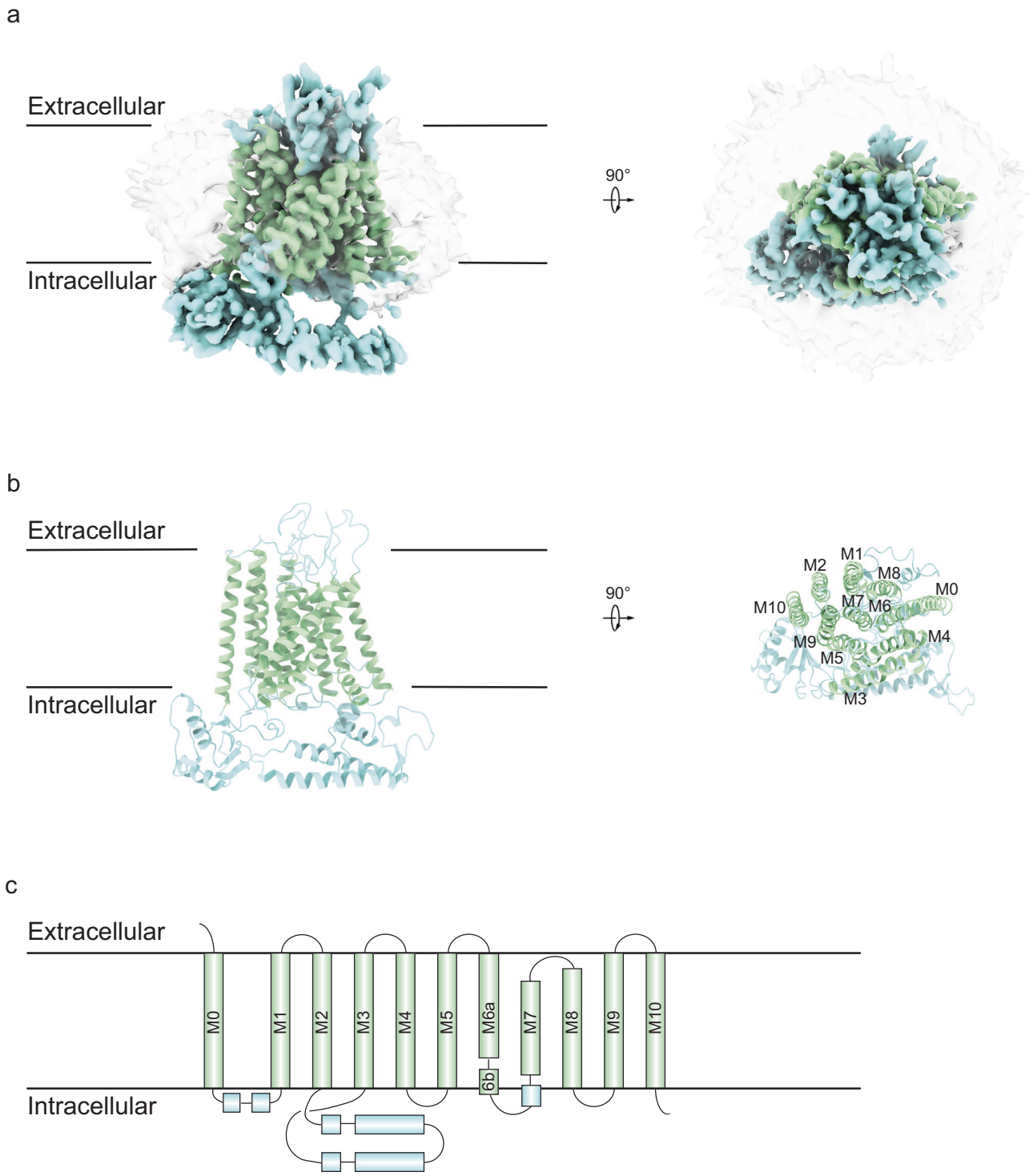

Fig. 1 | Cryo-EM structure of TMEM63C. a Side view (left) and top view (right) of TMEM63C EM density map at 3.56 Å resolution. The transmembrane region and soluble region are colored in green and blue respectively. The apparent micelle displays at a lower threshold. **b** Side view (left) and top view (right) of TMEM63C model. The color scheme is the same as the EM density map. **c** Topology of TMEM63C. The transmembrane helices are labeled M0 to M10.

https://doi.org/10.1038/s41467-023-42956-2

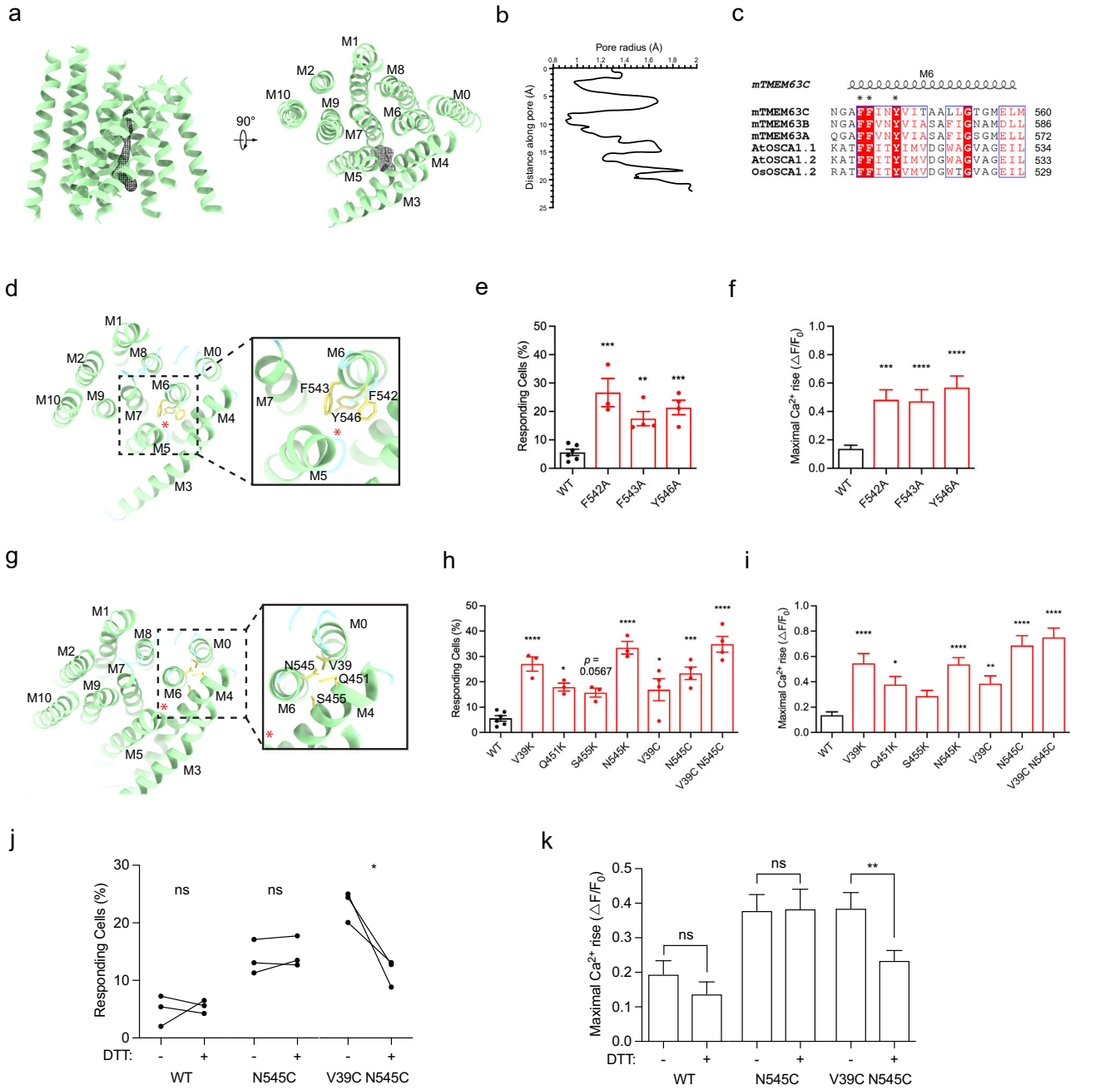

Fig. 2 | The pore profile of TMEM63C. a Top view (left) and side view (right) of TMEM63C transmembrane α-helices (green) and putative pore (black mesh). The pore is surrounded by α-helices M3 to M7. **b** The pore radius along distance of TMEM63C. **c** Sequence alignment of M6 transmembrane α-helix (coil) among TMEM63 and OSCA proteins. The three conserved residues F, F and Y are indicated with black asterisk above. **d** The three bulky pore-facing residues F542, F543 and Y546 (yellow) of TMEM63C in the pore. The position of the pore is indicated with red asterisk. **e** The responding ratio TMEM63C expressing cells to hypo-osmolality stress. WT ($n = 6$), F542A ($n = 3$, $p = 0.0002$), F543A ($n = 4$, $p = 0.0088$), Y546A ($n = 4$, $p = 0.0010$). **f** The maximal Ca^{2+} rise in response to hypo-osmolality stress. WT ($n = 563$), F542A ($n = 103$, $p = 0.0007$), F543A ($n = 192$, $p < 0.0001$), Y546A ($n = 214$, $p < 0.0001$). **g** The TMEM63C residues V39 in M0, Q451, S455 in M4 and N545 in M6 (yellow) outside the pore. **h** The responding ratio TMEM63C expressing cells to hypo-osmolality stress. WT ($n = 6$), V39K ($n = 3$, $p < 0.0001$), Q451K ($n = 3$, $p = 0.0144$), S455K ($n = 3$, $p = 0.0567$), N545K ($n = 3$, $p < 0.0001$), V39C ($n = 4$, $p = 0.0138$), N545C ($n = 4$, $p = 0.0001$), V39C N545C ($n = 4$, $p < 0.0001$). **i** The maximal Ca^{2+} rise in response to hypo-osmolality stress. WT ($n = 563$), V39K ($n = 163$, $p < 0.0001$), Q451K ($n = 194$, $p = 0.0161$), S455K ($n = 169$, $p = 0.3789$), N545K ($n = 241$, $p < 0.0001$), V39C ($n = 280$, $p = 0.0026$), N545C ($n = 306$, $p < 0.0001$), V39C N545C ($n = 265$, $p < 0.0001$). Data (**e**, **f**, **h**, **i**) are shown as mean ± SEM. $^{*}p < 0.05$; $^{**}p < 0.01$; $^{***}p < 0.001$; $^{****}p < 0.0001$; one-way ANOVA followed by Tukey's multiple comparisons test. **j**, **k** The channel activity of double mutant (V39C N545C) but not wild type or single mutant (N545C) TMEM63C decreased significantly in the presence of DTT. The responding cells (**j**) and maximal Ca^{2+} rise (**k**) in response to hypo-osmolality stress are shown. **j** WT DTT- ($n = 3$), WT DTT+ ($n = 3$), WT DTT- vs. DTT+ $p = 0.7983$, N545C DTT- ($n = 3$), N545C DTT+ ($n = 3$), N545C DTT- vs. DTT+ $p = 0.3968$, V39C N545C DTT− ($n = 3$), V39C N545C DTT+ ($n = 3$), V39C N545C DTT− vs. DTT+ $p = 0.0485$. **k** WT DTT− ($n = 156$), WT DTT+ ($n = 306$), WT DTT− vs. DTT+ $p = 0.3188$, N545C DTT− ($n = 476$), N545C DTT+ ($n = 413$), N545C DTT− vs. DTT+ $p = 0.9445$, V39C N545C DTT− ($n = 383$), V39C N545C DTT+ ($n = 630$), V39C N545C DTT− vs. DTT+ $p = 0.0036$. Data (**j**, **k**) are shown as mean ± SEM. $^{*}p < 0.05$; $^{**}p < 0.01$; ns not significant; paired (**j**) or unpaired (**k**) two-tailed t test. The corresponding plot information is in the source data.

https://doi.org/10.1038/s41467-023-42956-2

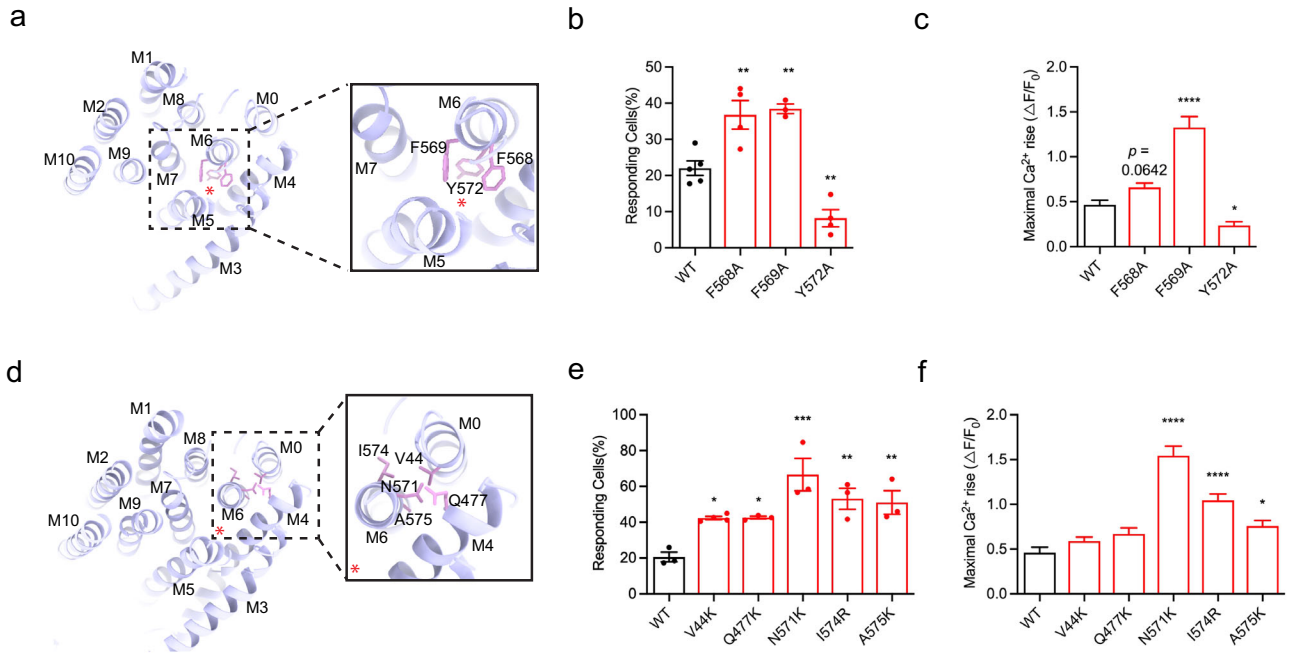

Fig. 3 | TMEM63B channel activity effected by the conserved residues identified in TMEM63C. a The three bulky pore-facing residues F568, F569 and Y572 (pink) of TMEM63B in the pore. The position of the pore is indicated with a red asterisk. The TMEM63B protein structure (purple) is predicted using Swiss-Model based on the TMEM63C structure. **b** The responding ratio of TMEM63B variants expressing cells to hypo-osmolality stress. WT ($n = 5$), F568A ($n = 4$, $p = 0.0041$), F569A ($n = 3$, $p = 0.0035$), Y572A ($n = 4$, $p = 0.0064$). **c** The maximal Ca^{2+} rise of TMEM63B variants in response to hypo-osmolality stress. WT ($n = 415$), F568A ($n = 335$, $p = 0.0642$), F569A ($n = 239$, $p < 0.0001$), Y572A ($n = 446$, $p = 0.0110$). **d** The TMEM63B residues V44 in M0, Q477K in M4, N571, I574 and A575 in M6 (pink) outside the pore. The position of the pore is indicated with a red asterisk. **e** The responding ratio of TMEM63B variants expressing cells to hypo-osmolality stress. WT ($n = 3$), V44K ($n = 4$, $p = 0.0254$), Q477K ($n = 3$, $p = 0.0352$), N571K ($n = 3$, $p = 0.0001$), I574R ($n = 3$, $p = 0.0024$), A575K ($n = 3$, $p = 0.0041$). **f** The maximal Ca^{2+} rise of TMEM63B variants in response to hypo-osmolality stress. WT ($n = 201$), V44K ($n = 205$, $p = 0.7111$), Q477K ($n = 133$, $p = 0.3850$), N571K ($n = 321$, $p < 0.0001$), I574R ($n = 195$, $p < 0.0001$), A575K ($n = 252$, $p = 0.0380$). Data (**b**, **c**, **e**, **f**) are shown as mean ± SEM. $^{*}p < 0.05$; $^{**}p < 0.01$; $^{***}p < 0.001$; $^{****}p < 0.0001$; one-way ANOVA followed by Tukey's multiple comparisons test. The corresponding plot information is in the source data.

model of TMEM63C. Similar to TMEM63C, we performed mutagenesis and functional assay for three highly conserved bulky residues located in the entry site of the pore. Alanine substitution of F568 and F569 on TM6 of TMEM63B led to increased channel activity, while Y572A reduced channel activity (Fig. 3a–c, Supplementary Fig. 5c). These results indicated although TMEM63 proteins share similar working mechanisms, there might be subtle differences to fulfill their functional varieties under physiological conditions.

In order to further confirm the critical roles of these conserved residues outside the pore identified in TMEM63C, we conducted measurements of channel activity using corresponding mutants in TMEM63B through calcium imaging. In line with our observation in TMEM63C, these mutants of TMEM63B demonstrated a higher responding ratio compared to the wild type. Particularly, substitution of residues on TM0 (V44), TM4 (Q477) with lysine increased the channel activity slightly, while substitution of residues on TM6 (N571, I574, A575) with lysine or arginine, increased the channel activity at least two times higher compared to that of wild type TMEM63B (Fig. 3d–f, Supplementary Fig. 5d). These findings suggested the generalizability of these key residues in influencing channel activity of TMEM63 proteins.

TMEM63C function as a monomer

Not like the structural observations of OSCA[25,27–29], the monomeric TMEM63C was observed in the cryo-EM structure. To investigate its physiological functional state, we performed pull-down assay by attaching GFP or FLAG at the C-terminus of TMEM63C, respectively. The cells were transfected by viruses of both TMEM63C-FLAG and TMEM63C-GFP together for overexpression. Following the same protocol as TMEM63C for structural studies, the harvested cells were solubilized in DDM before loading to GFP nanobody (GFP-Nb) beads and FLAG beads, respectively. After washing off the nonspecifically bound proteins, the beads were analyzed by western blotting. The results clearly show that the sample from GFP beads can only be detected by GFP antibody, whereas the sample from FLAG beads can only be detected by FLAG antibody, suggesting no dimer/oligomer was formed for TMEM63C (Fig. 4a). To exclude the possibility that the dimeric/oligomeric TMEM63C may be disassembled when extracted from the membrane, we purified cell membrane and performed crosslinking with glutaraldehyde (GA) before isolating by DDM. Consistently, no TMEM63C-FLAG/TMEM63C-GFP proteins have been observed for sample binding to GFP/FLAG beads (Fig. 4b). Besides, the TMEM63C-FLAG protein was expressed and crosslinked in the membrane without extraction. No dimer/oligomer band with higher molecular weight can be detected (Fig. 4c). These observations further demonstrated that TMEM63C is a monomer in the cell membrane, which is consistent with our structural observation.

Discussion

The TMEM63/OSCA family has been characterized as a mechanosensitive cation channel family in 2018[24,25]. The plant orthologues OSCAs have been shown to sense hyperosmotic stress as well as regulate water transpiration and root growth[24]. Several structures of OSCAs in similar closed states have been reported[25,27–29]. In contrast, the physiological roles of the TMEM63s remain unknown until 2020 when TMEM63B was identified as an osmosensor that is sensitive to hypotonic stress and required for hearing in mice[30], and a humidity sensor in 2022[36]. Considering the low sequence similarities

https://doi.org/10.1038/s41467-023-42956-2

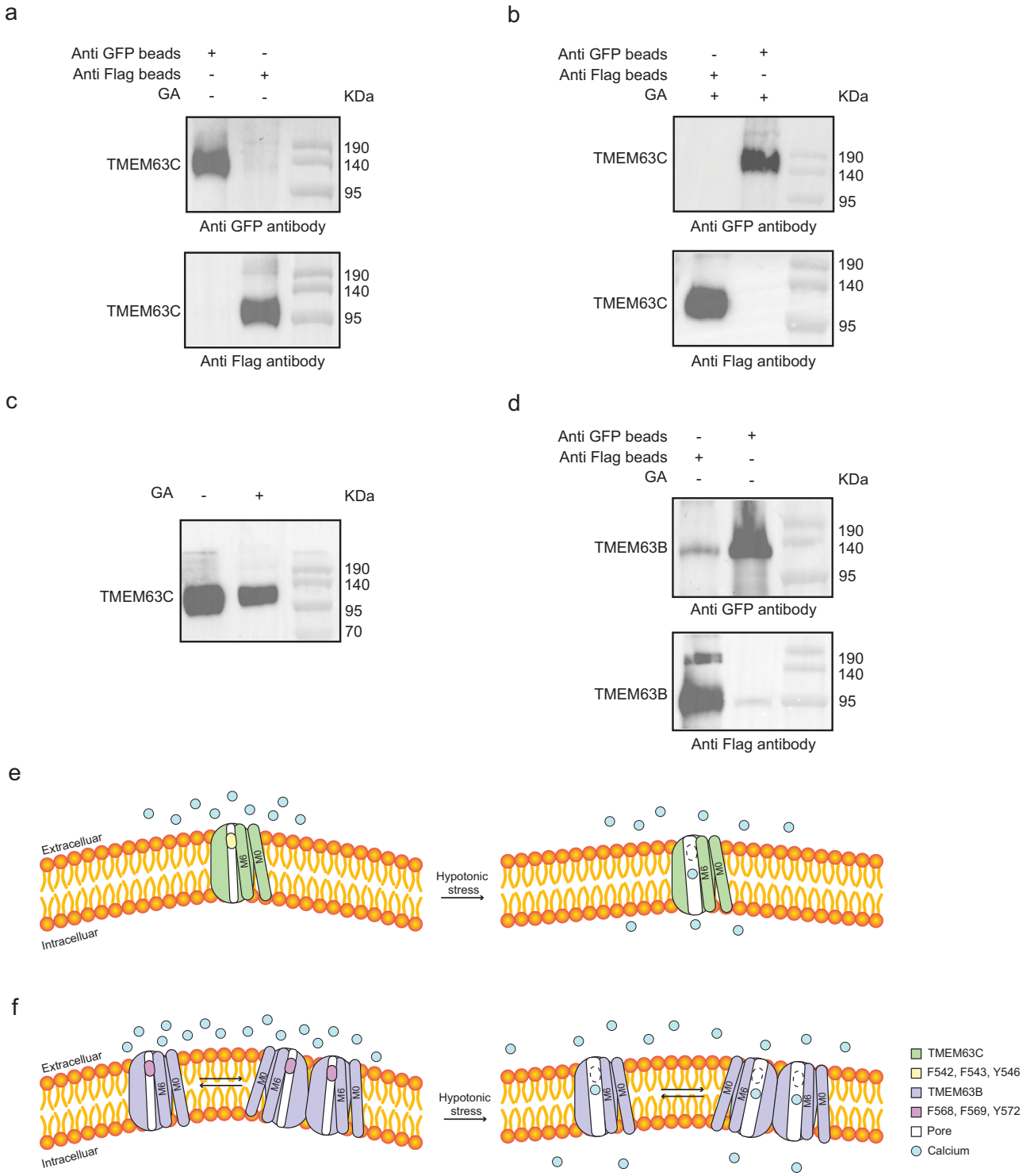

Fig. 4 | Native state of TMEM63C is a monomer. a Co-IP of TMEM63C without crosslinking. **b** Co-IP of TMEM63C with Glutaraldehyde (GA) crosslinking before extraction by using detergent. **c** Crosslink of TMEM63C-Flag in membrane with GA. **d** Co-IP of TMEM63B without crosslinking. All the assays are repeated at least 3 times with similar results. Proposed working model for TMEM63C (**e**) and TMEM63B (**f**). Calcium ion is indicated as blue circle.

(Supplementary Figs. 8, 9) and dramatically different responses to osmolality (hypo vs hyper) between TMEM63 and OSCAs, their molecular mechanisms are expected to be different.

In this study, we determined high-resolution structure of TMEM63C, which closely resembles that of hTMEMA (PDB: 8GRS; PDB: 8EHW) and hTMEM63B (PDB: 8EHX) reported recently[43,44], exhibiting an RMSD of less than 1.4 Å for pruned atom pairs, less than 6.2 Å for all pairs (Supplementary Fig. 6). Notably, the 11 transmembrane α-helices (TM0-TM10) display conserved structures with slight shift observed in TM0, TM3, TM4, and TM10. Additionally, TM10 of TMEM63C forms a longer helix by extending two turns in the cytoplasmic side. The major difference comes from TM6b, which presents different swing angles between TM0 and TM4 due to the flexible linker between TM6a and TM6b. While TM6b in other structures are closer to TM0, it is pushed

to the middle of TM0 and TM4 because of the shift of TM0 to TM6 in TMEM63C (Supplementary Fig. 6). The intracellular region, including the loop between TM2 and TM3, and the C-terminus, shows lower resolution among all four structures probably due to the flexibility. Additionally, we identified two non-protein densities within our cryo-EM map of TMEM63C, which are likely composed of lipids, and may contribute to the modulation of mechanosensitive ion channels gating[45,46]. These lipid densities are surrounded by specific residues in TM5 and TM9, situated in close proximity to the lipid observations made in the structures of hTMEM63A and hTMEM63B[44] (Supplementary Fig. 3c).

In combination with structural analyses and functional assay, we identified three highly conserved residues in TMEM63B/C that serve as a gate to regulate channel activity. In addition, our mutagenesis results suggested that the coupling of TM0 and TM6 played critical roles in opening the channel for ion transport. Previous studies[25] have suggested that MSCs sense mechanical force through membrane tension and distortion. Upon stimulated by mechanical forces, membrane will be distorted and generate a thinner region surrounding MSC. Membrane thinning could cause tilting of peripheral transmembrane helices (TM0 in TMEM63 proteins), and then trigger the conformational changes of pore-forming transmembrane helices (TM6 in this case). In this study, we further demonstrated the coupling of TM0 and TM6 is indispensable for the channel activity of TMEM63C, which could be a general principle for TMEM63 proteins, and even TMEM63/OSCA family proteins. Moreover, similar to previous studies[30], we noticed the delayed response of TMEM63 to hypotonic stress. Such delayed response was also observed in TRPC5 response to hypotonic stimulation, suggesting it is not unique for TMEM63 channels[47]. Hypotonic stimulation can trigger various signaling pathways, including the production of arachidonic acid metabolites and reactive oxygen species (ROS)[48]. These intracellular lipid metabolites or other signal molecules induced by hypotonic stress may also regulate the channel activity, contributing to a delayed and inconsistent calcium response. More works are needed to unravel the underlying mechanisms behind the observed delayed response and further enhance our understanding of TMEM63 function during hypotonic stress conditions.

Intriguingly, different from its homology OSCAs, TMEM63C functions as a monomer, which is confirmed by both cryo-EM structure and biochemical experiments. In principle, oligomerization states should not affect the channel function of TMEM63 since each monomer contains an intact ion permeation pore. In fact, even for the structurally homologous proteins, TMEM16A[31,32] and OSCAs[24,25,27–29], which form homodimers in cryo-EM structures, each monomer contains an intact ion permeation pore. We notice that several residues in the cytoplasmic region, which contribute to the dimerization of the AtOSCA1.1 by hydrogen bonding[25], are not conserved in TMEM63 (Supplementary Fig. 9), suggesting that the monomeric state of TMEM63, at least TMEM63C, may be physiological.

Although sharing high sequence similarity, TMEM63B showed dramatically higher activity than TMEM63C. The activity differences may be attributed to the oligomerization state of TMEM63B and TMEM63C, which is partially supported by our cryo-EM studies of purified mouse TMEM63B. 2D classification of TMEM63B particles indicated that some 2D averages showed clear C2 symmetry from top/bottom views, indicating the existence of dimeric TMEM63B (Supplementary Fig. 7). In contrast, 2D averages of TMEM63C only showed monomeric but not dimeric states (Supplementary Fig. 1d). To further verify the dimeric TMEM63B observed in cryo-EM study, we performed a pull-down assay to examine the oligomerization states of TMEM63B in cells following the same protocol for TMEM63C (Fig. 4d). The results suggested the existence of oligomeric (probably dimeric) TMEM63B in physiological states, which is in line with a previous study[49]. The differences of oligomerization in TMEM63B and TMEM63C may contribute to variation of their channel activity.

On the basis of the observation in structure and channel activity, the dimerization may provide a novel strategy to regulate the channel activity of TMEM63. Although the monomeric TMEM63 contains an intact pore region and can conduct channel function independently, the activity is relatively low. Dimerization of TMEM63 may require conformational adjustments in a way that facilitates channel open probability[50], thus producing a higher channel activity in TMEM63B (Fig. 4e, f). Future studies are needed to investigate channel activities of monomeric and dimeric TMEM63 protein to confirm this hypothesis. It would be interesting to find out whether the oligomerization states of TMEM63B will affect its mechanosensory functions and whether oligomerization is a form of regulation to fine-tune the sensitivity of ion channels.

Methods

Protein expression and purification

The mouse TMEM63C (Uniprot ID: Q8CBX0) was cloned into vector pEG BacMam with a C-terminus TEV cutting site and GFP tag. Bacmids were generated from DH10Bac bacteria, and baculovirus was produced and amplified in Sf9 cells according to the Bac-to-Bac protocol. The HEK293S cells were cultured in FreeStyle medium (Gibco #12338018), 2% FBS (Gibco, #10270106), 5% CO_2, and 40% humidity at 37 °C. 500 ml HEK293S with a density of 2.0×10^6 cells/ml were infected by baculovirus to a volume ratio 1:100 (baculovirus: HEK293S). 8 h after viral infection, 10 mM Sodium butyrate (Sigma #303410) was added. HEK293S cells were collected after another 48 h.

Cells were resuspended with buffer 50 mM Tris pH 7.0, 150 mM NaCl, 10% glycerol, and protein inhibitor cocktail, and then broken through dounce homogenizer. Membrane proteins were extracted using 1% DDM (Anatrace #D310A) and 0.1% CHS (Anatrace #CH210) for 2 h at 4 °C. The insoluble fraction was removed via centrifugation at $24{,}400 \times g$ for 45 min. The supernatant was incubated with pre-equilibrated GFP nanobody coupled CNBr-Activated Sepharose 4B resin (Cytiva #17043001) for an hour at 4 °C, followed by three times wash with buffer 50 mM Tris pH 7.0, 150 mM NaCl, 10% glycerol, 0.02% DDM, and 0.002% CHS. The protein was released from the resin through 3 h of TEV digestion at 4 °C to remove the C-terminus GFP tag. Subsequently, 500 ul concentrated protein was injected to Superdex 200 increase 10/300 column for size-exclusion chromatography with buffer 50 mM Tris pH 7.0, 150 mM NaCl, 0.002% LMNG (Anatrace #NG310), and 0.0004% CHS. The peak fraction was verified by SDS-PAGE and concentrated to 1 mg/ml for cryo-EM analysis.

Similarly, the mouse TMEM63B (Uniprot ID: Q3TWI9) was cloned into vector pEG BacMam with a GFP tag. 1 L HEK293S cells were infected by corresponding TMEM63B baculovirus with a volume ratio of 1:50 and cultured at 37 °C overnight. Sodium butyrate (10 mM) was applied, and the cells were cultured at 30 °C for 48 h before harvesting. The cells were resuspended with buffer containing 20 mM Hepes, pH8.0, 150 mM NaCl, 2 mM TCEP, 10% glycerol and protease inhibitor. After emulsification for 10 min, the membrane protein was extracted with 1% DDM and 0.1% CHS rotating for 2 h at 4 °C. The insoluble fraction was removed via centrifugation at $39{,}000 \times g$ for 45 min. The protein was purified with GFP resin and released through thrombin digestion. The size-exclusion chromatography was performed using Superdex 200 increase 10/300 column with buffer 50 mM Hepes pH 8.0, 150 mM NaCl, 2 mM TCEP, 0.02%LMNG, and 0.002%CHS.

Cryo-EM sample preparation and data collection

4 μL purified protein was placed on the holy-carbon grids (Quantifoil Au R1.2/1.3, 300 mesh), which were glow-discharged for 30 s. The grids were blotted for 4 s with blot force 0, at 100% humidity, 4 °C, and plunge-frozen into liquid ethane using Vitrobot Mark IV (Thermo Fisher Scientific).

11,058 movies were collected on 300 kV Titan Krios (Thermo Fisher Scientific) equipped with a GIF BioQuantum and K3 camera

(Gatan) using software EPU (Thermo Fisher Scientific). Each movie contained 40 fractions with a total dose of ~50 $e^-/Å^2$ for 4.5 s exposure time. The pixel size was 1.06 Å per pixel, and the defocus ranged from −1.0 µm to −2.5 µm.

Cryo-EM data processing
All movies were motion-corrected, dose-weighted, and gain-normalized using MotionCor2[51]. The contrast transfer function (CTF) of non-does-weighted micrographs was estimated by Gctf[52]. 8,754,694 particles were picked by Gautomatch with 256 × 256 box size, extracted from dose-weighted micrographs in RELION[53], and then cleaned up by using 2D classification and heterogeneous refinement in cryoSPARC[54]. The well-sorted particles generated a reference map, which worked as a reference to enrich the particles[55] from the Gautomatch picked raw particles through seed facilitated 3D classification[56]. The raw particles were split into several portions, and each portion was combined with seed particles. These combined particles were classified using referenced and biased maps, followed by removing duplicates. The enriched 1,417,132 particles were further cleaned up by resolution gradient 3D classification[56]. To obtain the reference for the resolution gradient, a map was generated using 958,924 particles after 2D classification and seed facilitated 3D classification, then combined with the low-pass filtered 10 Å and 20 Å map. Both the seed facilitated 3D classification and resolution gradient 3D classification were done through cryoSPARC heterogeneous refinement. The 258,464 particles yielded a 3.56 Å map using local and global CTF refinement, local refinement and DeepEMhancer[57].

Model building
The initial model of TMEM63C was predicted with AlphaFold[58], and fitted into cryo-EM map in Chimera[59]. The model was manually adjusted in COOT[60] and subsequently refined with real space refinement in PHENIX[61] iteratively. The transmembrane α-helix region of the model was identified unambiguously, while the loop region was adjusted based on the remaining density. The intracellular region (211-400) from AlphaFold prediction fits into the fragmented density. The TMEM63C model is validated by the Molprobity score[62] and Ramachandran plots in PHENIX. Additionally, the structure of TMEM63B is predicted using homology modeling according to the TMEM63C model in Swiss-Model[63].

Co-IP
Two constructs TMEM63C with a C-terminus GFP tag and TMEM63C with a C-terminus Flag tag, were co-expressed in the HEK293S cells. Cells were collected and washed via centrifugation at 2000 × *g* for 10 min, followed by resuspending with lysis buffer 20 mM Hepes pH 7.0, 150 mM NaCl, 10% glycerol, and an additional protein inhibitor cocktail. 1% DDM and 0.1% CHS were added to lysis cells, and extract membrane protein at 4 °C for 2 h. After removing the cell pellet at 16,000 × *g* for 30 min, the supernatant was divided into two parts that incubated with GFP resin and Flag resin at 4 °C overnight separately. The GFP resin and Flag resin were washed at 1000 × *g* for 5 min four times. Each protein coupled resin was analyzed by SDS-PAGE and western blot using both anti-GFP and anti-Flag antibodies. The same protocol was applied for TMEM63B, except the pH value of lysis buffer changed to 8.0.

Crosslink
The TMEM63C is expressed in the HEK293S cells, which were collected and resuspended with lysis buffer 20 mM Hepes pH 7.0, 150 mM NaCl, 10% glycerol, and an additional protein inhibitor cocktail. Cells were broken through dounce homogenizer, and the pellet was removed via centrifugation at 4300 × *g* for 30 min. From the supernatant, the membrane was obtained via ultracentrifugation at 200,000 × *g* for an hour. The membrane was resuspended with lysis buffer and crosslinked with 0.02% glutaraldehyde at 4 °C for 30 min. The 50 mM Tris 7.0 was applied to stop the crosslink reaction. The crosslinked membrane was analyzed by SDS-PAGE and western blot.

SDS-PAGE and western blot
The protein samples were added to a 12% Bis-Tris gel system for electrophoresis. PVDF membranes (Merck Millipore #IPVH00010) were applied to blot the protein sample at constant 400 mA, 4 °C for 2 h, and blocked with 5% milk TBST buffer. The membranes were incubated with the primary antibodies GFP tag rabbit polyAb (Proteintech #50430-2-AP; 1:10,000 dilution in TBST) or monoclonal anti-Flag M2 antibody produced in mouse (Sigma #F1804; 1:10,000 dilution in TBST) was incubated overnight at 4 °C, followed by three times TBST wash. The respective secondary antibodies Goat Anti-Rabbit IgG (TransGen #HS101-01; 1:10,000 dilution in TBST) or Goat Anti-Mouse IgG (TransGen #HS201-01; 1:10,000 dilution in TBST) were incubated for an hour at room temperature, followed by three times TBST wash. The signal was detected with supersignal west pico plus chemiluminescent substrate (Thermo Fisher Scientific #34580) using ChemiDoc Imaging Systems (Bio-rad).

Cytoplasmic Ca^{2+} measurements
The cytoplasmic Ca^{2+} influx was monitored by free calcium indicator GCaMP6f as previously reported[30,49]. TMEM63C/TMEM63B-P2A-GCaMP6f vectors were transfected into N2a cells mounted on the coverslip. Forty hours after transfection, the cells were perfused with isotonic extracellular solution containing 70 mM NaCl, 5 mM KCl, 1 mM $CaCl_2$, 1 mM $MgCl_2$, 10 mM HEPES, and 10 mM glucose (pH 7.4 adjusted with NaOH, 300 mOsm/liter adjusted with mannitol). The isotonic solution was exchanged to 170 mOsm/liter hypotonic solution without changing the ionic concentrations by a peristaltic pump (Longer Precision Pump, BT100-2J, China) at a constant speed. The osmolarity was measured by a vapor pressure osmometer (Wescor, Vapro 5600). The cytoplasmic calcium fluorescence was recorded at 1 Hz for 10 min by the Hamamatsu digital imaging camera (Hamamatsu, C11440-22U) at RT (24 ± 2°C) using 488 nm illumination. The change of fluorescence was normalized by the ratio of real-time intensity (Ft) relative to the initial value (F0). The cells with Ft/F0 > 1.5 were considered as positive responses to hypotonic challenge.

Statistical analysis
All data are presented as means ± SEM. Statistical analyses were performed using the GraphPad Prism software (version 8.0) (GraphPad Software Inc) and analyzed using one-way ANOVA, followed by Tukey's multiple comparisons test, paired or unpaired *t* test, if not otherwise stated. *p* values less than 0.05 were considered statistically significant. $^*p < 0.05$; $^{**}p < 0.01$; $^{***}p < 0.001$; $^{****}p < 0.0001$. $p \geq 0.05$ was denoted as "ns".

Reporting summary
Further information on research design is available in the Nature Portfolio Reporting Summary linked to this article.

Data availability
Cryo-EM density map of TMEM63C has been deposited in the Electron Microscopy Data Bank under accession code EMD-36759 (TMEM63C). Atomic coordinate has been deposited in the Protein Data Bank under accession code 8K0B (TMEM63C). All other data are available from the corresponding authors upon request. Source data are provided with this paper.

References
1. Kung, C. A possible unifying principle for mechanosensation. *Nature* **436**, 647–654 (2005).

2. Gillespie, P. G. & Müller, U. Mechanotransduction by hair cells: models, molecules, and mechanisms. *Cell* **139**, 33–44 (2009).
3. Jin, P., Jan, L. Y. & Jan, Y. N. Mechanosensitive ion channels: structural features relevant to mechanotransduction mechanisms. *Ann. Rev. Neurosci.* **43**, 207–229 (2020).
4. Sukharev, S. I., Blount, P., Martinac, B., Blattner, F. R. & Kung, C. A large-conductance mechanosensitive channel in E. coli encoded by mscL alone. *Nature* **368**, 265–268 (1994).
5. Sukharev, S. I., Martinac, B., Arshavsky, V. Y. & Kung, C. Two types of mechanosensitive channels in the Escherichia coli cell envelope: solubilization and functional reconstitution. *Biophys. J.* **65**, 177–183 (1993).
6. Sukharev, S., Betanzos, M., Chiang, C. S. & Robert Guy, H. The gating mechanism of the large mechanosensitive channel MscL. *Nature* **409**, 720–724 (2001).
7. Batiza, A. F., Kuo, M. M. C., Yoshimura, K. & Kung, C. Gating the bacterial mechanosensitive channel MscL in vivo. *Proc. Natl. Acad. Sci. USA* **99**, 5643–5648 (2002).
8. Bootha, I. R. & Blount, P. The MscS and MscL families of mechanosensitive channels act as microbial emergency release valves. *J. Bacteriol.* **194**, 4802–4809 (2012).
9. Maingret, F., Fosset, M., Lesage, F., Lazdunski, M. & Honoré, E. TRAAK is a mammalian neuronal mechano-gated K+ channel. *J. Biol. Chem.* **274**, 1381–1387 (1999).
10. Franks, N. P. & Honoré, E. The TREK K 2P channels and their role in general anaesthesia and neuroprotection. *Trends Pharmacol. Sci.* **25**, 601–608 (2004).
11. Coste, B. et al. Piezo proteins are pore-forming subunits of mechanically activated channels. *Nature* **483**, 176–181 (2012).
12. Coste, B. et al. Piezo1 and Piezo2 are essential components of distinct mechanically activated cation channels. *Science* **330**, 55–60 (2010).
13. Murthy, S. E., Dubin, A. E. & Patapoutian, A. Piezos thrive under pressure: mechanically activated ion channels in health and disease. *Nat. Rev. Mol. Cell Biol.* **18**, 771–783 (2017).
14. Lehnert, B. P., Baker, A. E., Gaudry, Q., Chiang, A. S. & Wilson, R. I. Distinct roles of TRP channels in auditory transduction and amplification in Drosophila. *Neuron* **77**, 115–128 (2013).
15. Zhang, W., Yan, Z., Jan, L. Y. & Jan, Y. N. Sound response mediated by the TRP channels NOMPC, NANCHUNG, and INACTIVE in chordotonal organs of Drosophila larvae. *Proc. Natl. Acad. Sci. USA* **110**, 13612–13617 (2013).
16. Walker, R. G., Willingham, A. T. & Zuker, C. S. A Drosophila mechanosensory transduction channel. *Science* **287**, 2229–2234 (2000).
17. Yan, Z. et al. Drosophila NOMPC is a mechanotransduction channel subunit for gentle-touch sensation. *Nature* **493**, 221–225 (2013).
18. Jin, P. et al. Electron cryo-microscopy structure of the mechanotransduction channel NOMPC. *Nature* **547**, 118–122 (2017).
19. Lingueglia, E. ENAC, Degenerins, ASICs, and related channels. in *Encyclopedia of Biophysics* 664–674 (Springer, 2013). https://doi.org/10.1007/978-3-642-16712-6_363 (2013).
20. Kellenberger, S. & Schild, L. Epithelial sodium channel/degenerin family of ion channels: a variety of functions for a shared structure. *Physiol. Rev.* **82**, 735–767 (2002).
21. Pan, B. et al. TMC1 forms the pore of mechanosensory transduction channels in vertebrate inner ear hair cells. *Neuron* **99**, 736–753.e6 (2018).
22. Pan, B. et al. TMC1 and TMC2 are components of the mechanotransduction channel in hair cells of the mammalian inner ear. *Neuron* **79**, 504–515 (2013).
23. Jia, Y. et al. TMC1 and TMC2 proteins are pore-forming subunits of mechanosensitive ion channels. *Neuron* **105**, 310–321.e3 (2020).
24. Murthy, S. E. et al. OSCA/TMEM63 are an evolutionarily conserved family of mechanically activated ion channels. *Elife* **7**, e41844 (2018).
25. Zhang, M. et al. Structure of the mechanosensitive OSCA channels. *Nat. Struct. Mol. Biol.* **25**, 850–858 (2018).
26. Yuan, F. et al. OSCA1 mediates osmotic-stress-evoked Ca2+ increases vital for osmosensing in Arabidopsis. *Nature* **514**, 367–371 (2014).
27. Liu, X., Wang, J. & Sun, L. Structure of the hyperosmolality-gated calcium-permeable channel OSCA1.2. *Nat. Commun.* **9**, 1–9 (2018).
28. Jojoa-Cruz, S. et al. Cryo-EM structure of the mechanically activated ion channel OSCA1.2. *Elife* **7**, e41845 (2018).
29. Maity, K. et al. Cryo-EM structure of OSCA1.2 from Oryza sativa elucidates the mechanical basis of potential membrane hyperosmolality gating. *Proc. Natl. Acad. Sci. USA* **116**, 14309–14318 (2019).
30. Du, H. et al. The cation channel TMEM63B is an osmosensor required for hearing. *Cell Rep.* **31**, 107596 (2020).
31. Dang, S. et al. Cryo-EM structures of the TMEM16A calcium-activated chloride channel. *Nature* **552**, 426–429 (2017).
32. Paulino, C., Kalienkova, V., Lam, A. K. M., Neldner, Y. & Dutzler, R. Activation mechanism of the calcium-activated chloride channel TMEM16A revealed by cryo-EM. *Nature* **552**, 421–425 (2017).
33. Feng, S. et al. Cryo-EM studies of TMEM16F calcium-activated ion channel suggest features important for lipid scrambling. *Cell Rep.* **28**, 567–579.e4 (2019).
34. Jeong, H. et al. Structures of the TMC-1 complex illuminate mechanosensory transduction. *Nature* **610**, 796–803 (2022).
35. Clark, S., Jeong, H., Posert, R., Goehring, A. & Gouaux, E. Structure of C. elegans TMC-2 complex suggests roles of lipid-mediated subunit contacts in mechanosensory transduction. *bioRxiv* 2023.08.16.553618. https://doi.org/10.1101/2023.08.16.553618 (2023).
36. Li, S., Li, B., Gao, L., Wang, J. & Yan, Z. Humidity response in Drosophila olfactory sensory neurons requires the mechanosensitive channel TMEM63. *Nat. Commun.* **13**, 1–12 (2022).
37. Li, Q. & Montell, C. Mechanism for food texture preference based on grittiness. *Curr. Biol.* **31**, 1850–1861.e6 (2021).
38. Yan, H. et al. Heterozygous variants in the mechanosensitive ion channel TMEM63A result in transient hypomyelination during infancy. *Am. J. Hum. Genet.* **105**, 996–1004 (2019).
39. Marques, M. C., Albuquerque, I. S., Vaz, S. H. & Bernardes, G. J. L. Overexpression of osmosensitive Ca2+-permeable channel TMEM63B promotes migration in HEK293T cells. *Biochemistry* **58**, 2861–2866 (2019).
40. Schulz, A. et al. Analysis of the genomic architecture of a complex trait locus in hypertensive rat models links Tmem63C to kidney damage. *Elife* **8**, e42068 (2019).
41. Jojoa-Cruz, S., Burendei, B., Lee, W.-H. & Ward, A. B. Structure of mechanically activated ion channel OSCA2.3 reveals mobile elements in the transmembrane domain. *bioRxiv* 2023.06.15.545135. https://doi.org/10.1101/2023.06.15.545135 (2023).
42. Chovancova, E. et al. CAVER 3.0: a tool for the analysis of transport pathways in dynamic protein structures. *PLoS Comput. Biol.* **8**, 23–30 (2012).
43. Zhang, M., Shan, Y., Cox, C. D. & Pei, D. A mechanical-coupling mechanism in OSCA/TMEM63 channel mechanosensitivity. *Nat. Commun.* **14**, 3943 (2023).
44. Zheng, W. et al. TMEM63 proteins function as monomeric high-threshold mechanosensitive ion channels. Article TMEM63 proteins function as monomeric high-threshold mechanosensitive ion channels. *Neuron* 1–16. https://doi.org/10.1016/j.neuron.2023.07.006 (2023).
45. Battle, A. R. et al. Lipid-protein interactions: lessons learned from stress. *Biochim. Biophys. Acta Biomembr.* **1848**, 1744–1756 (2015).

46. Romero, L. O. et al. Dietary fatty acids fine-tune Piezo1 mechanical response. *Nat. Commun.* **10**, 1–14 (2019).
47. Gomis, A., Soriano, S., Belmonte, C. & Viana, F. Hypoosmotic- and pressure-induced membrane stretch activate TRPC5 channels. *J. Physiol.* **586**, 5633–5649 (2008).
48. Hoffmann, E. K., Lambert, I. H. & Pedersen, S. F. Physiology of cell volume regulation in vertebrates. *Physiol. Rev.* **89**, 193–277 (2009).
49. Wu, D. et al. A splicing-dependent ER retention signal regulates surface expression of the mechanosensitive TMEM63B cation channel. *J. Biol. Chem.* **299**, 102781 (2023).
50. Haselwandter, C. A. & Phillips, R. Connection between oligomeric state and gating characteristics of mechanosensitive ion channels. *PLoS Comput. Biol.* **9**, e1003055 (2013).
51. Zheng, S. Q. et al. MotionCor2: anisotropic correction of beam-induced motion for improved cryo-electron microscopy. *Nat. Methods* **14**, 331–332 (2017).
52. Zhang, K. Gctf: real-time CTF determination and correction. *J. Struct. Biol.* **193**, 1–12 (2016).
53. Kimanius, D., Dong, L., Sharov, G., Nakane, T. & Scheres, S. H. W. New tools for automated cryo-EM single-particle analysis in RELION-4.0. *Biochem. J.* **478**, 4169–4185 (2021).
54. Punjani, A., Rubinstein, J. L., Fleet, D. J. & Brubaker, M. A. CryoSPARC: algorithms for rapid unsupervised cryo-EM structure determination. *Nat. Methods* **14**, 290–296 (2017).
55. Su, C. C. et al. A 'Build and Retrieve' methodology to simultaneously solve cryo-EM structures of membrane proteins. *Nat. Methods* **18**, 69–75 (2021).
56. Yuan, Y. et al. Cryo-EM structure of human glucose transporter GLUT4. *Nat. Commun.* **13**, 1–8 (2022).
57. Sanchez-Garcia, R. et al. DeepEMhancer: a deep learning solution for cryo-EM volume post-processing. *Commun. Biol.* **4**, 874 (2021). 2020.06.12.148296.
58. Jumper, J. et al. Highly accurate protein structure prediction with AlphaFold. *Nature* **596**, 583–589 (2021).
59. Pettersen, E. F. et al. UCSF Chimera—a visualization system for exploratory research and analysis. *J. Comput. Chem.* **25**, 1605–1612 (2004).
60. Emsley, P., Lohkamp, B., Scott, W. G. & Cowtan, K. Features and development of Coot. *Acta Crystallogr. D Biol. Crystallogr.* **66**, 486–501 (2010).
61. Adams, P. D. et al. PHENIX: a comprehensive Python-based system for macromolecular structure solution. *Acta Crystallogr. D* **66**, 213–221 (2010).
62. Chen, V. B. et al. MolProbity: all-atom structure validation for macromolecular crystallography. *Acta Crystallogr. D Biol. Crystallogr.* **66**, 12–21 (2010).
63. Waterhouse, A. et al. SWISS-MODEL: homology modelling of protein structures and complexes. *Nucleic Acids Res.* **46**, W296–W303 (2018).

Acknowledgements

We thank Yifan Cheng for critical reading of the manuscript, Kaihua Zhang, and Caleigh Azumaya for the help at the early stage of protein purification. All cryo-EM data were collected at the Biological Cryo-EM Center at HKUST, generously supported by a donation from the Lo Kwee Seong Foundation. This project is supported by grants from Hong Kong Research Grants Council (ECS26101919, GRF16103321, GRF16102822 and C6001-21EF), Southern Marine Science and Engineering Guangdong Laboratory (Guangzhou) (SMSEGL20SC01), Guangdong Basic and Applied Basic Research Foundation (2021A1515012460), Shenzhen Special Fund for Local Science and Technology Development Guided by Central Government (2021Szvup140), HKUST VPRDO 30 for 30 Research Initiative Scheme, and HKUST start-up and initiation grants to S.D. This work is also supported by grants from the National Key R&D Program of China (2019YFA0801603 to Y.S.S.); the National Natural Science Foundation of China (32330044, 32170951 to Y.S.S., 82101393 to D.W., 81920108017, 82130036 to Y.X.); the Natural Science Foundation of Jiangsu Province (BE2019707 to Y.S.S., BK20210008 to D.W., BE2020620 to Y.X.); Jiangsu Provincial Medical Key Discipline (ZDXK202216 to Y.X.); Special Fund for Science and Technology Innovation Strategy of Guangdong Province (2021B0909050004 to Y.S.S.); the Fundamental Research Funds for the Central Universities (021414380533 to Y.S.S.); the Jiangsu Planned Projects for Postdoctoral Research Funds (2021K462C to D.W.); the STI2030-Major Projects (2022ZD0211800 to Y.X.). D.Y. and J.D. are supported by LKS fellowships.

Author contributions

S.D. and Y.S.S. conceived the study. Y.Q., J.D., W.T.L., K.C.C., and Y.W. performed protein purification and biochemical experiments. Y.Q., D.Y., J.D., Y.Z., and S.D. prepared cryo-samples and collected cryo-EM datasets, Y.Q., D.Y., and J.D. processed images, built the atomic model. Y.Q. performed Co-IP assay. D.W., C.Y., and Y.X. performed calcium imaging. Y.W., Y.S.S., and S.D. supervised experiments and data analysis. Y.Q. and S.D. prepared figures and wrote the manuscript with input from all the others. All authors contributed to data analysis and manuscript preparation. All authors contributed to data analysis and manuscript preparation.

Competing interests

The authors declare no competing interests.

Additional information

Supplementary information The online version contains supplementary material available at https://doi.org/10.1038/s41467-023-42956-2.

Correspondence and requests for materials should be addressed to YongQiang Wang, Yun Stone Shi or Shangyu Dang.

Peer review information *Nature Communications* thanks Duanqing Pei and Zhiqiang Yan for their contribution to the peer review of this work. A peer review file is available.

Reprints and permissions information is available at http://www.nature.com/reprints

Publisher's note Springer Nature remains neutral with regard to jurisdictional claims in published maps and institutional affiliations.

Open Access This article is licensed under a Creative Commons Attribution 4.0 International License, which permits use, sharing, adaptation, distribution and reproduction in any medium or format, as long as you give appropriate credit to the original author(s) and the source, provide a link to the Creative Commons license, and indicate if changes were made. The images or other third party material in this article are included in the article's Creative Commons license, unless indicated otherwise in a credit line to the material. If material is not included in the article's Creative Commons license and your intended use is not permitted by statutory regulation or exceeds the permitted use, you will need to obtain permission directly from the copyright holder. To view a copy of this license, visit http://creativecommons.org/licenses/by/4.0/.

© The Author(s) 2023